Article

Fractal Dimension Characteristics of the Soil Cracking Process When Saline-Alkali Soil Is Mixed with Hippophae Roots

Lichuang Jin [1], Shuai Zhang [1,*] and Yingjie Xu [2]

1   College of Geoscience and Surveying Engineering, China University of Mining and Technology (Beijing), Beijing 100083, China
2   School of Civil Engineering, Xuchang University, No. 88 Bayi Rd, Xuchang 461000, China
*   Correspondence: zhangshuaicumtb@163.com

Abstract: Fractal analysis is an effective tool to describe real world phenomena. Water evaporation from the soil surface under extreme climatic conditions, such as drought, causes salt to accumulate in the soil, resulting in soil salinization, which aggravates soil shrinkage, deformation, and cracking. Hippophae is an alkali tolerant plant that is widely grown in Northwest China. Laboratory drying shrinkage tests of Saline-Alkali soil samples with 0%, 0.5%, 1%, and 2% concentrations of hippophae roots were carried out to study the effect of hippophae roots on the evaporation and cracking of Saline-Alkali soil and to determine variation characteristics of the soil samples' fractal dimensions. A series of changes in the cracking parameters of Saline-Alkali soil were obtained during the cracking period. Based on fractal theory and the powerful image processing function of ImageJ software, the relationships between samples' cracking process parameters were evaluated qualitatively and quantitatively. The experimental results show that the residual water contents of Saline-Alkali soil samples with 0%, 0.5%, 1%, and 2% concentrations of hippophae roots were 2.887%, 4.086%, 5.366%, and 6.696%, respectively. The residual water content of Saline-Alkali soil samples with 0.5% and 1% concentrations of hippophae roots increased by 41.53% and 85.87%, respectively; the residual water content of the sample with a 2% concentration of hippophae roots was 131.94% higher than that of the sample without hippophae roots. The final crack ratios of Saline-Alkali soil samples with 0%, 0.5%, 1%, and 2% concentrations of hippophae roots were 21.34%, 20.3%, 18.93%, and 17.18%, respectively. The final crack ratios of Saline-Alkali soil samples with 0.5%, 1%, and 2% concentrations of hippophae roots reduced by 4.87%, 11.29%, and 19.49%, respectively, compared with that of the sample without hippophae roots. Fractal dimensions at the end of cracking were 1.6217, 1.5656, 1.5282, and 1.4568, respectively. Fractal dimensions increased with an increase in the crack ratio and with a decrease in water content. The relationship between water content and fractal dimension can be expressed using a quadratic function. Results indicate that hippophae roots can effectively inhibit the cracking of Saline-Alkali soil and improve its water holding capacity.

Keywords: fractal dimension; Saline-Alkali soil; cracking; water content; ImageJ software

1. Introduction

Soil pollution is a worldwide crisis, which often leads to changes in soil environments [1]. Soil salinization seriously affects agricultural production and sustainable land use [2]. This problem is particularly prominent in arid and semi-arid areas [3,4], which accelerates soil degradation. Previous studies have shown that soil's water holding capacity is negatively correlated with salt ions [5], so drought may increase the adverse effects of salt on plant nutrition [6]. Sometimes, it can cause a nutrient imbalance in farmland, resulting in abnormal plant growth [7]. In areas with a shortage of high-quality water or a high demand for industrial and urban water, salty soda water is often used for irrigation, which indirectly increases the risk of soil salinization [8,9]. At the same time, water in soil cracks can promote salt leaching [10]. High-salinity wastewater has long-term effects on the soil's

hydraulic properties and flow paths [11]. Salt conditions not only cause chemical and physical changes in clay, but also have an important influence on the crack morphology of dry clay [12]. Experiments have shown that soil's hydration rate is related to its soluble salt content, but independent of particle size distribution [13]. Relevant field and laboratory tests were carried out to study the effect of salt on soil cracking, and an online method for the rapid determination of salt content in soda-saline soil was proposed [14]. Studies have shown that soil salinity plays a leading role in the growth of cracks, showing a positive correlation [15]. Crack lengths increase with an increase in the salt content of the pore water in the soil [16,17]. Figure 1 shows the hazards of Saline-Alkali soil.
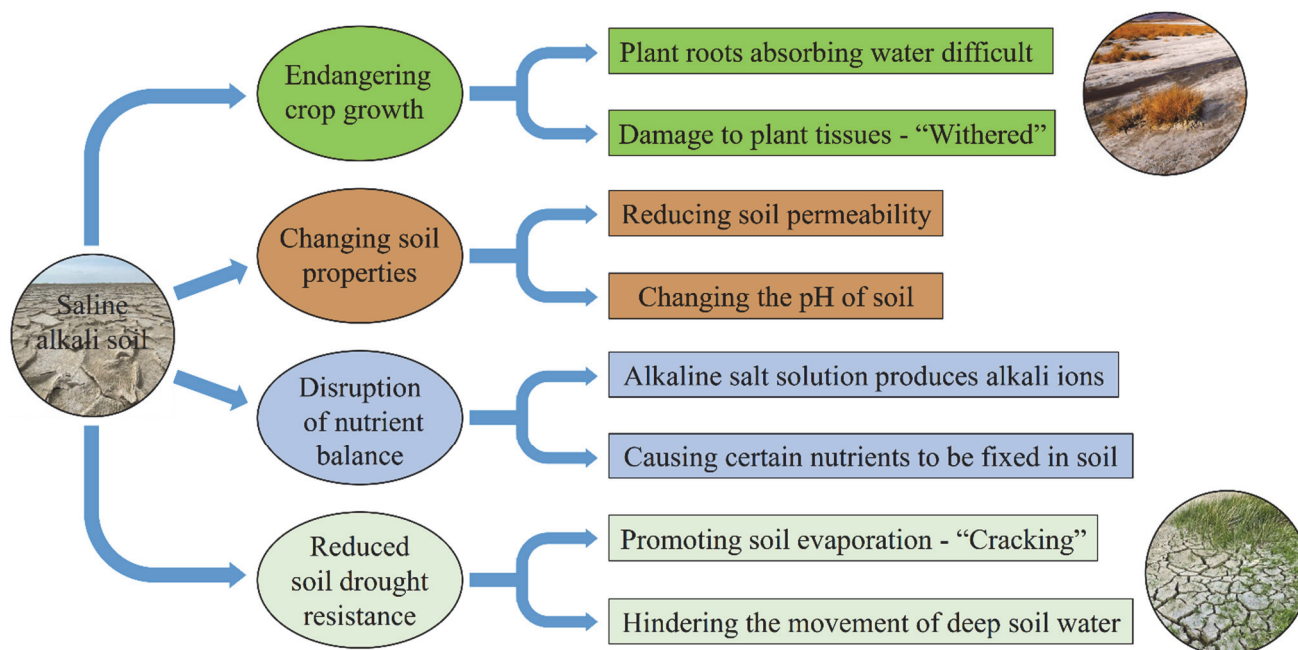
Figure 1. The hazards of Saline-Alkali soil.

Dry cracking of the soil's surface is a common phenomenon associated with soil–atmosphere interaction [18]. Soil exposed to the environment for a long time is damaged by multiple factors [19], including wind, rainfall, sunshine, and other factors, which damage the soil's integrity, leading to a reduction in soil moisture. The dry season is an important factor that facilitates the formation of soil cracks [20]. Soil cracking has a series of negative effects. For example, clay material has a wide range of environmental applications and is often used as cover for landfills. However, soil cracks caused by drought not only cause clay to lose its barrier function, but also creates channels for pollutant transport [21,22], causing surface water and groundwater pollution [23,24]. Slope soil cracking seriously affects a slope's stability, and is the main cause of slope instability [25,26]. In fields of farmland, soil cracking has an adverse impact on irrigation efficiency and reduces crop yields [27]. Many methods are used to characterize soil structure, most of which are based on fractal theory [28]. Fractal dimension mainly describes the most important parameters of fractal. Fractal geometry can be used to analyze the characteristics of soil particle size distribution and the spatial variability of fractal and soil structure parameters using statistical methods [29]. Relevant studies have found that the soil fractal dimension is related to soil particle size. The fractal dimension increased with the fine soil content [30,31]. Lu et al. analyzed the change law of particle size characteristics and the main sliding direction of landslides based on the fractal dimension, and documented the trend that the fractal dimension increases in the main sliding direction [32]. The fractal dimension is used to quantify the complex geometry of soil cracking patterns [33]. An algorithm to determine the fractal dimension of crack edge by digitizing photos of soil cracking samples was proposed, which is helpful in characterizing soil cracks [23]. This study examined

the effect of adding different concentrations of hippophae roots to Saline-Alkali soil on its evaporation cracking. The evaporation and cracking processes of Saline-Alkali soil with different concentrations of hippophae roots were simulated using laboratory tests. Based on image processing technology, the fractal dimension of soil samples was quantitatively obtained, and changes in alkaline soil water content and evaporation rates were analyzed. Finally, the relationships between fractal dimension and crack ratio, and fractal dimension and the water content of alkaline soil samples were evaluated.

2. Materials and Methods

2.1. Test Materials

The soil used in this experiment was from the Aksu City, Xinjiang Uygur Autonomous Region, a typical Saline-Alkali area in China, with an arid climate and low annual rainfall. The annual precipitation is 75–80 mm, and the annual evaporation is 1200–1500 mm. The sampling depth was 20 cm below the surface. The basic physical properties of this soil are shown in Table 1.

**Table 1.** Basic physical properties of the soil.

Soil Properties	Values
Specific gravity (g/cm^3)	2.56
Particle composition	
Clay (<0.002 mm)	56.5
Silt (0.002–0.075 mm)	33.7
Sand (>0.075 mm)	9.8
Liquid limit (%)	37.2
Plasticity limit (%)	18.3
Plasticity Index	17.9
Main chemical composition	
K^+ (mg/g)	0.14
Na^+ (mg/g)	6.56
Ca^{2+} (mg/g)	1.25
Cl^- (mg/g)	2.77
CO_3^{2-} (mg/g)	1.16
SO_4^{2-} (mg/g)	1.37
Salinity (mg/g)	26.5
pH	8.52

Hippophae roots were selected as the additive material in this study. Hippophae is a deciduous shrub characterized by drought, wind, and sand resistance; it can survive on Saline-Alkali land. Hippophae is widely planted in Northwest China for desert greening and Saline-Alkali land improvement. Therefore, hippophae plays an important role in soil and water conservation. Hippophae roots were crushed in a grinder to approximately 5 mm long with a 2 mm diameter. Saline-Alkali soil samples were air-dried, ground, and weighed. Next, hippophae roots were added to Saline-Alkali soil samples; the mass ratios of hippophae roots to soil were 0%, 0.5%, 1%, and 2%. Finally, samples were placed in four rectangular parallelepiped glass containers with inner diameters of 25 cm × 25 cm × 4 cm. Slurries were prepared with supersaturated water contents of 125% and mixed evenly. Then, mixed slurries were placed in a natural state until water loss and cracking occurred.

2.2. Image and Data Processing

During the experiment, a high-precision platform scale was used to test changes in soil samples' water content and the cracking of the samples was monitored using a digital camera; changes in water content and the extent of cracking were recorded for samples with different concentrations of hippophae roots. Next, water content change data and images of cracking were input into a computer. ImageJ software, an open-source software based on Java [34], which can quickly complete grayscale and binary image processing

to obtain basic image information (such as resolution, color mode, color channel, unit, pixel distribution, etc.) was used to process images. ImageJ software's image threshold segmentation function can realize area measurement and quantitative analysis of porosity. A schematic diagram of the sample device and processing process is shown in Figure 2.
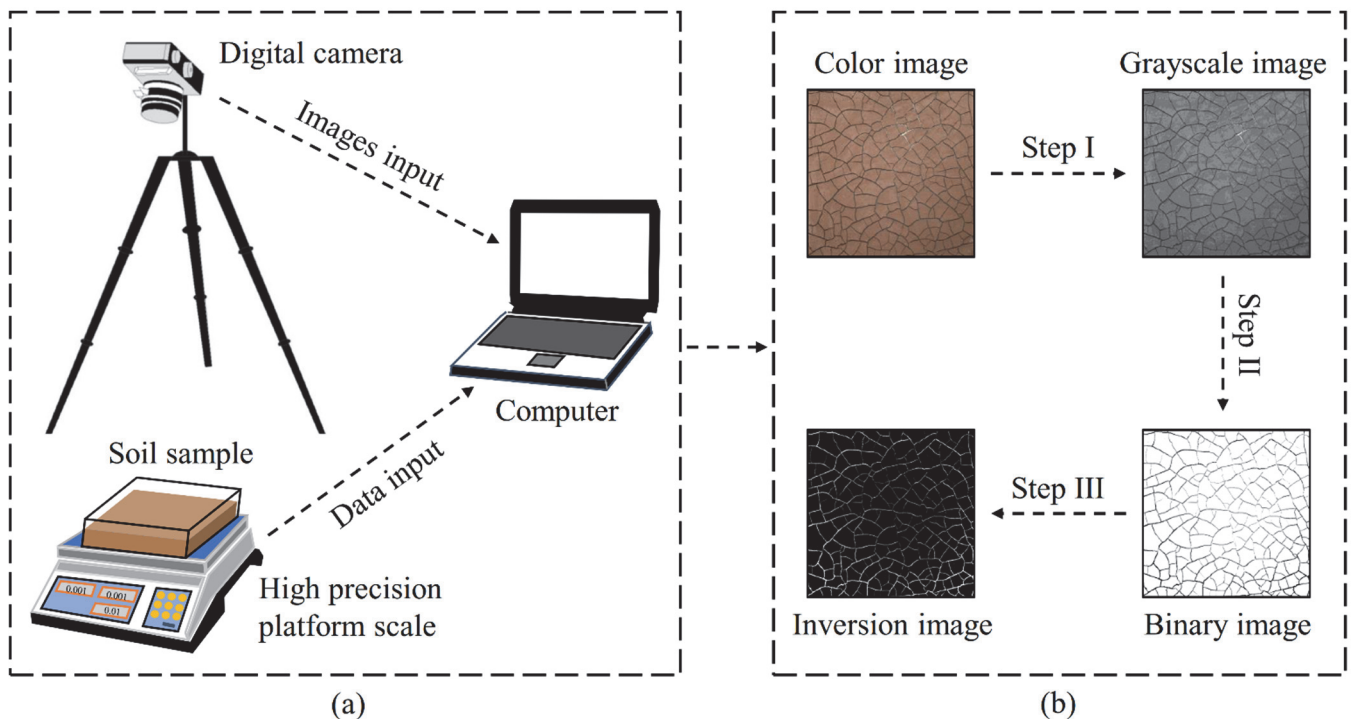
Figure 2. A schematic diagram of the sample device and processing process: (**a**) Data and images acquisition system; (**b**) Image processing.

Pixels of the original images recorded using a digital camera were composed of three colors: red (*R*), green (*G*), and blue (*B*). To realize an accurate quantitative analysis of the cracks, image processing was carried out to highlight the cracks, as shown in Figure 2. This study's image processing can be summarized in three steps.

Step I: Color images were converted into grayscale images using Formula (1).

$$Gray = R \times 0.4 + G \times 0.4 + B \times 0.2 \tag{1}$$

where *Gray* represents grayscale; the value ranges from 0 to 255.

Step II: Grayscale images were converted into binary images using Formula (2). The threshold segmentation method binarized the image to further distinguish the cracks from other parts of the soil surface. Using the grayscale threshold value to distinguish the cracks from uncracked areas. Pixels were defined as a crack if the grayscale exceeded the threshold; otherwise, they were in uncracked areas. Assuming that the grayscale value of the original pixel is $f(x, y)$ and the threshold value is *T*, the specific formula for calculating the binary pixel value is as follows:

$$f(x,y) = \begin{cases} 1, & f(x,y) \geq T \\ 0, & f(x,y) < T \end{cases} \tag{2}$$

where $f(x, y)$ represents the grayscale value of the image after the binarization process, and *T* represents the threshold.

Step III: Binary images were converted into inversion images using ImageJ software's inverse function so that each image's foreground became its background, and its background became its foreground. Obviously, this was a one-to-one mapping, where the pixel

value 0 became 255, 1 became 254 . . . , 254 became 1, and 255 became 0. The fracture morphology was more obvious when the binarization image was inverted.

Fractal dimension, as a statistic to describe the complexity of a geometric shape. The larger the fractal dimension of an image, the more "roughness" and complex the image is. The fractal dimension of regular objects can be directly calculated using Formula (3).

$$D = -\frac{logN}{log\varepsilon} \tag{3}$$

where D represents the fractal dimension, N represents the unit length, and ε represents the reduction ratio of unit length compared with the original graphics. However, cracks on the soil surface are extremely irregular, so the box counting method was used to calculate the fractal dimension of surface cracks. The specific formula is shown in Formula (4).

$$D_B = -\lim_{S \to 0} \frac{log(C)}{log(S)} \tag{4}$$

where D_B represents the fractal dimension of the box counting method, S represents the box size, and C represents count boxes covered by the crack trace under the set box size. The water content of a soil sample can be defined as:

$$\omega = \frac{m - m_0}{m_0} \tag{5}$$

where ω is the rate of water loss (%), m is the mass of the soil sample before drying (g), and m_0 is the mass of the soil sample after drying (g). The evaporation rate can be calculated using Formula (6).

$$E = \frac{\Delta m}{S \bullet \Delta t} \tag{6}$$

where E is the evaporation rate of soil samples (g/dm^2/h), Δm is the change in soil mass at equal intervals (g), S is the area of sample surface (dm^2), and Δt is the time interval of evaporation (h). The crack ratio of a sample can be defined as:

$$\delta = \frac{\sum S_c}{S} \tag{7}$$

where δ is the ratio of crack, S is the surface area of the soil sample, and S_c is the surface crack area of the soil. The measurement of area is essentially image segmentation. Common methods of image segmentation include automatic segmentation and manual segmentation. The quality of image segmentation directly affects the calculation accuracy of area.

3. Results

*3.1. Change in Water Content and Evaporation Rate*

Figure 3 shows the relationship between water content and time of Saline-Alkali soil samples. The change in water content can be divided into three stages. Stage I represents the decrease rapidly of water content. During stage I, the Saline-Alkali soil samples without roots and with a 2% concentration of hippophae roots lasted for 76 and 82 h, respectively. Stage II represents the decrease slowly of water content. The Saline-Alkali soil sample without hippophae roots and with a 2% concentration of hippophae roots lasted for 94 and 98 h, respectively. Stage III represents the residual of water content. The water content of Saline-Alkali soil samples tended to be constant at the end of this stage. The residual water content of Saline-Alkali soil samples with 0%, 0.5%, 1%, and 2% concentrations of hippophae roots were 2.887%, 4.086%, 5.366%, and 6.696%, respectively. The residual water content of Saline-Alkali soil samples with 0.5% and 1% concentrations of hippophae roots increased by 41.53% and 85.87%, respectively; the sample with a 2% concentration of roots was 131.94% higher than that of the Saline-Alkali soil sample without hippophae roots.

These results indicate that under the conditions of experimental design, the greater the hippophae roots concentration, the greater the residual water content.
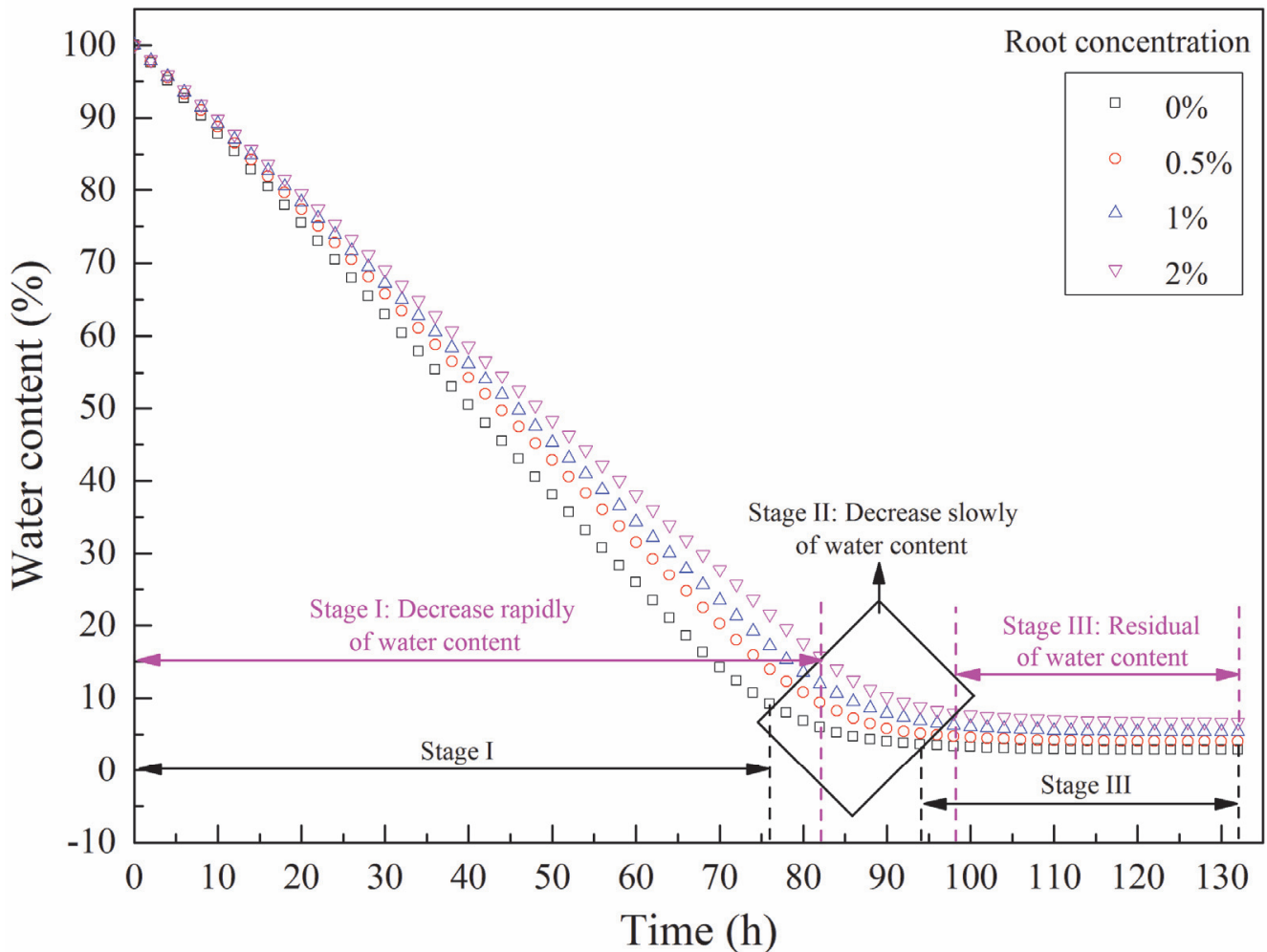
Figure 3. The relationship between water content and time of Saline-Alkali soil samples.

Figure 4 shows the relationship between evaporation rates and time of Saline-Alkali soil samples. In stage I, the evaporation rate was stable and higher than that in stages II and III. During stage I, soil pores were filled with water, which moved rapidly to the sample surface through capillary action, resulting in a high evaporation rate. The evaporation rate decreased with an increase in hippophae roots concentration. Four groups of Saline-Alkali soil samples entered stage II between 66 h and 78 h, successively. The evaporation rate slowed at this stage. As a large amount of water evaporation in stage I, capillary action gradually weakened or even stopped. As a result, the evaporation rate of water decreased significantly. Stage III represents the residual evaporation rate. At this stage, there was residual water in Saline-Alkali soil samples, and the structure of Saline-Alkali soil samples tended to be stable.
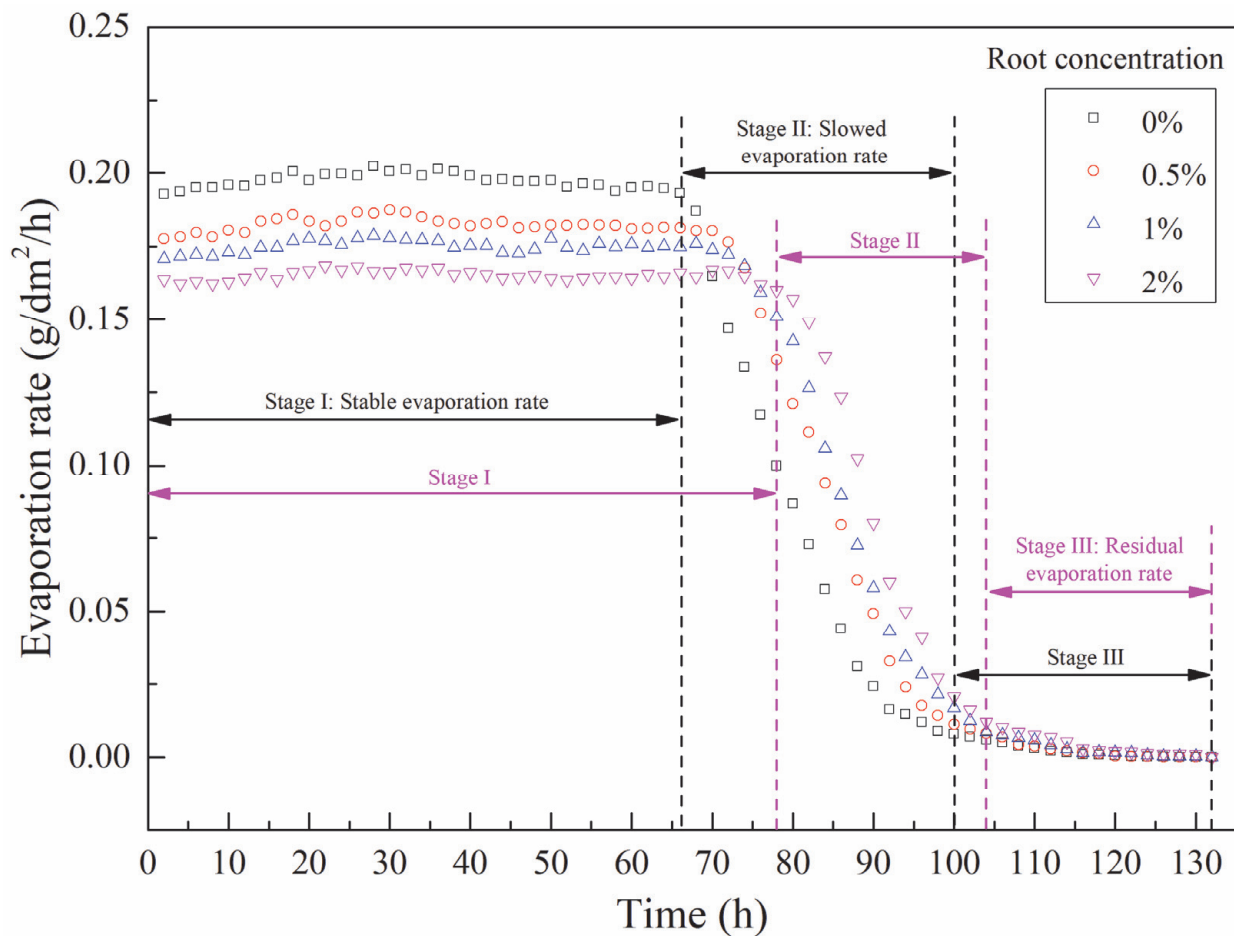
Figure 4. The relationship between evaporation rates and time of Saline-Alkali soil samples.

3.2. Changes in Crack Ratio and Fractal Dimension

After binarizing the cracking pictures of Saline-Alkali soil samples, the fractal dimensions of the crack surfaces were calculated using the box counting method. Table 2 shows the fractal dimensions of Saline-Alkali soil samples at the beginning and end of cracking.
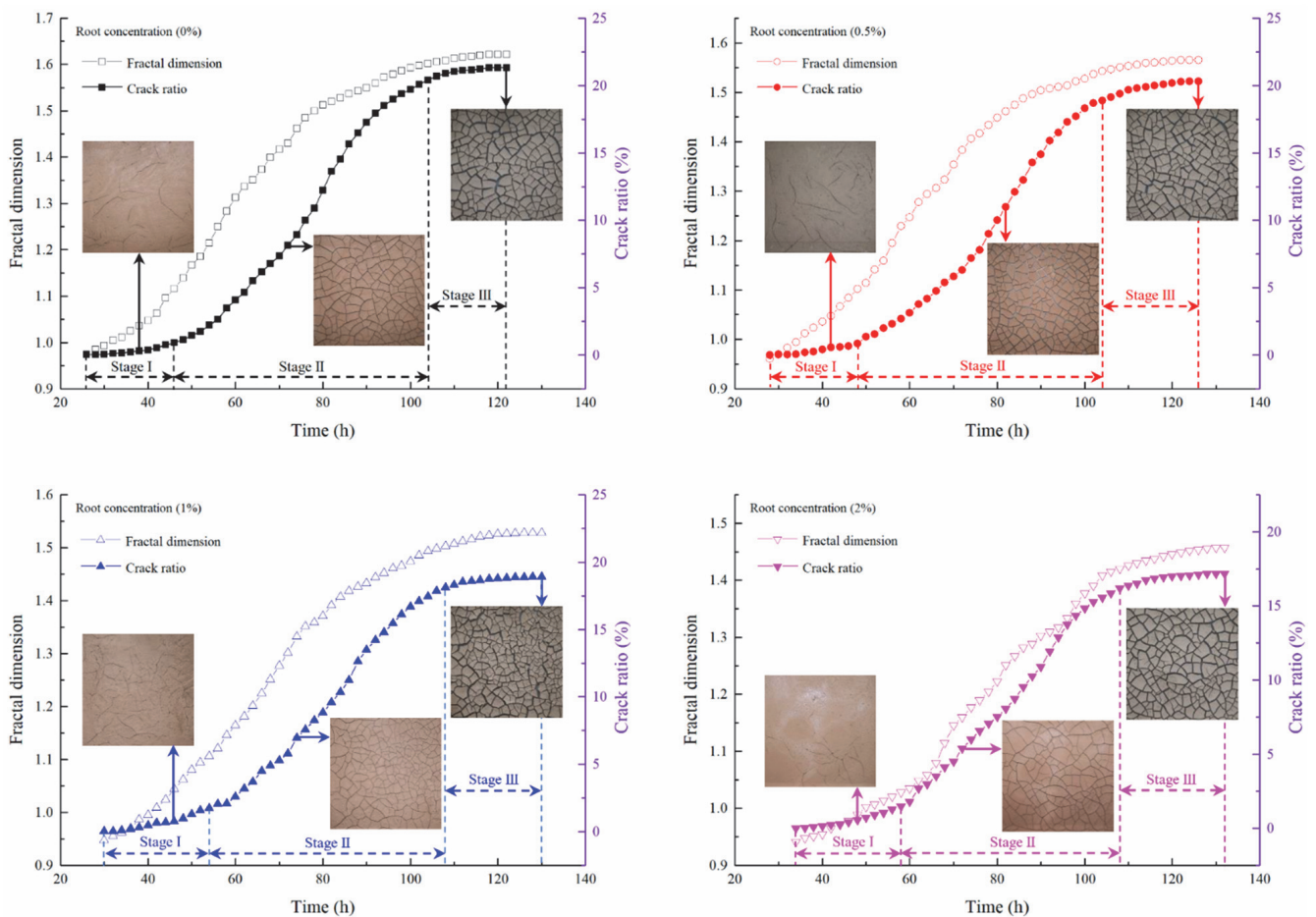
Table 2. Fractal dimensions of Saline-Alkali soil samples at the beginning and end of cracking.

Group	Box Size									D_B
	2	**3**	**4**	**6**	**8**	**12**	**16**	**32**	**64**	
Count 1 (S)	9362	5699	4129	2666	1971	1376	1031	563	310	0.9749
Count 2 (S)	5872	3474	2464	1574	1176	818	613	352	204	0.9602
Count 3 (S)	17,144	10,508	7628	5005	3787	2668	2023	1118	614	0.9478
Count 4 (S)	6561	4094	3032	2018	1544	1053	811	436	246	0.9414
Count 1 (E)	497,154	234,234	138,561	67,700	41,457	21303	13,557	4868	1803	1.6217
Count 2 (E)	431,982	208,839	126,111	63,351	39,540	20,855	13,445	4956	1903	1.5656
Count 3 (E)	400,536	195,593	119,005	60,865	38,546	20,835	13,614	5206	1958	1.5282
Count 4 (E)	264,178	131,407	81,099	42,434	27,478	15,325	10,248	4095	1657	1.4568

Note: (S)–represents count boxes covered by crack traces of samples at the beginning of cracking; (E)–represents count boxes covered by crack traces of samples at the ending of cracking.

Figure 5 shows the relationship between fractal dimension and crack ratios with time of Saline-Alkali soil samples and illustrates that the entire cracking process can be divided in three stages. Stage I reflects the slow cracking of Saline-Alkali soil samples; the sample with no hippophae roots was earliest to crack, at 26 h, and the sample with a 2% hippophae roots concentration was the last to crack, at 34 h. Stage I for the four Saline-Alkali soil

samples ended between 46 h and 58 h. At this stage, crack morphology was characterized by short length and narrow width. Stage II reflects the accelerated cracking of Saline-Alkali soil samples. The soil samples significantly shrank and cracked as water content decreased. During this stage, the cracking and expansion speed of the primary cracks accelerated, microcracks formed continuously from the primary cracks, and cracks staggered, forming a network. Stage III reflects the end of cracking. The cracking of Saline-Alkali soil samples tended to stabilize, and cracks' morphology characteristics included large width and depth. The final crack ratios of Saline-Alkali soil samples with 0%, 0.5%, 1%, and 2% concentration of hippophae roots were 21.34%, 20.3%, 18.93%, and 17.18%, respectively. The final crack ratios of Saline-Alkali soil samples with 0.5%, 1%, and 2% concentrations of hippophae roots were reduced by 4.87%, 11.29%, and 19.49%, respectively, compared with that of the soil sample without hippophae roots. Combining Table 2 and Figure 5, it can be noted that the fractal dimensions of Saline-Alkali soil samples containing 0%, 0.5%, 1%, and 2% of roots at initial cracking were 0.9749, 0.9602, 0.9478, and 0.9414, respectively, and that the fractal dimensions at the end of cracking were 1.6217, 1.5656, 1.5282, and 1.4568, respectively. The final fractal dimensions of Saline-Alkali soil samples with 0.5%, 1%, and 2% concentrations of hippophae roots were reduced by 3.46%, 5.77%, and 10.17%, respectively, compared with the soil without hippophae roots. This indicates that adding hippophae roots to Saline-Alkali soil effectively reduced the fractal dimension of cracks, and (within the concentration range set in the experiment) that the fractal dimension of samples' cracking negatively correlated with the concentration of hippophae roots.

Figure 5. The relationship between fractal dimension and crack ratio with time of Saline-Alkali soil samples.

4. Discussion

4.1. Application of Fractal Theory

Many researchers have studied fractal analysis as an effective tool to describe real-world phenomena. Fractal dimension can effectively characterize the complexity of shale pore structure and the degree of micropore development [35]. The surface area and pore volume of siliceous shale are positively correlated with fractal dimension [36]. In mathematics, the coupled system of fractional differential equations is applied to a variety of mathematical models [37]. Fractal and fractional derivatives are applied to ordinary differential equations to establish a model of partial differential equations [38]. In the environmental protection field, the fractal dimension reflects the time structure of the ratio of PM10 and PM2.5 (hot spots for environmental protection), which is helpful in determining pollution sources [39]. In the engineering field, fractal dimension is used to analyze the space-time structural characteristics of rock mass fractures formed by mining activities [40]. In geochemistry, traditional exploration data analysis technology can only draw strong geochemical anomalies, whereas the concentration area fractal model can draw a variety of geochemical anomaly maps, which is conducive to the determination of drilling targets [41]. The element concentration–distance method, a new fractal method, was developed to separate geochemical anomalies from backgrounds. The element concentration–distance model can effectively distinguish the background area from geochemical anomalies [42]. In medical applications, fractal dimension analysis of bone tissue has been introduced as an alternative method to study alveolar bone quality [43]. Moreover, changes in soil properties are reflected by the fractal dimension of soil particle size distribution, which can be used as an evaluation index of soil property changes, and indirectly reflects the degree of desertification [44]. Additionally, fractal mathematical modeling is important in the study of the relationship between soil fractal and solute transport parameters [45], and the proportion of apparent soil water distribution can be described using fractal parameters [46].

As previously mentioned, the practical applications of fractal dimension are interesting and extensive. In this paper, the fractal dimension changes in surface cracks of soil samples containing different concentrations of hippophae roots during cracking were analyzed. The relationship between fractal dimension and crack ratio, fractal dimension and water content will be discussed next.

4.2. Analysis of Fractal Dimension

4.2.1. Relationship between Crack Ratio and Fractal Dimension

Figure 6 shows the relationship between crack ratio and fractal dimension. The crack ratio and fractal dimension of Saline-Alkali soil without roots were the largest, and the crack ratio and fractal dimension of Saline-Alkali soil with 2% hippophae roots concentration were the smallest, which indicated that the larger the crack ratio, the larger the fractal dimension. Crack widths continued to increase with the gradual cracking of Saline-Alkali soil samples. In samples with hippophae roots, the friction and adhesion between the roots and the soil needed to be overcome during the cracking process. A higher concentration of hippophae roots meant a greater probability of roots being in the cracks and intersecting the cracks at any angle, creating greater friction and adhesion to be overcome during the cracking process; as a result, crack widths on the surfaces of samples with a higher concentration of hippophae roots were reduced. The fractal dimension represents the irregularity of crack morphology; it increased with an increase in the crack ratio. The larger the root concentration, the stronger the resistance to cracking. Therefore, in this study, the fractal dimension and the root concentration show a negative correlation.
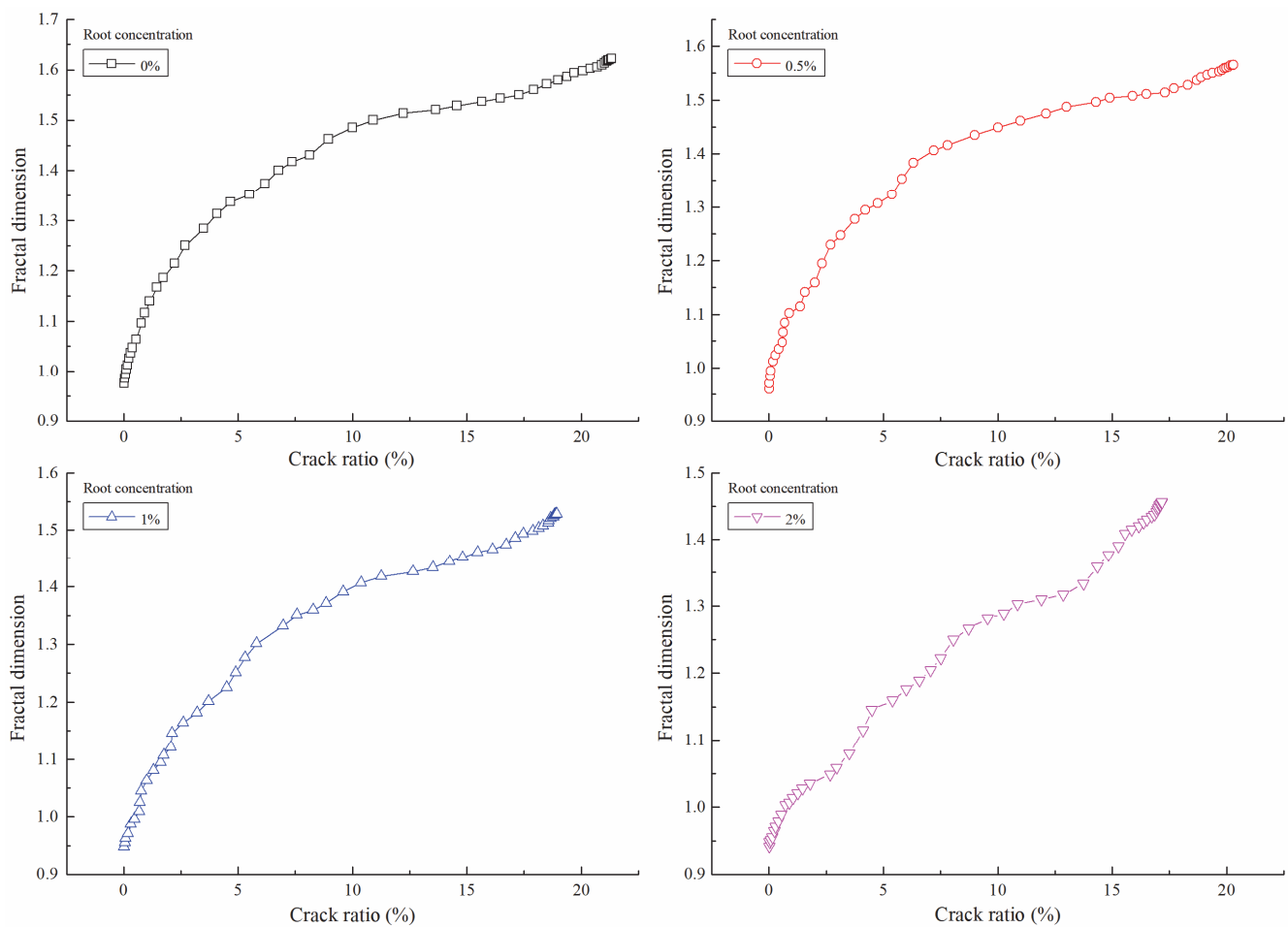
Figure 6. Relationship between crack ratio and fractal dimension.

4.2.2. Relationship between Water Content and Fractal Dimension

Figure 7 shows the relationship between water content and fractal dimension. The larger the water content in the Saline-Alkali soil sample, the smaller the fractal dimension of the sample's surface cracks, indicating that the fractal dimension of the crack surface negatively correlated with the soil's water content, which is consistent with results of previous research [47]. The relationship between water content and fractal dimension can be expressed using a quadratic function. The fractal dimension increased with a decrease in water content. The judgment coefficient R^2 of the fitting equations of the four types of soil samples were greater than 0.976, indicating the accuracy of the fitting effect.
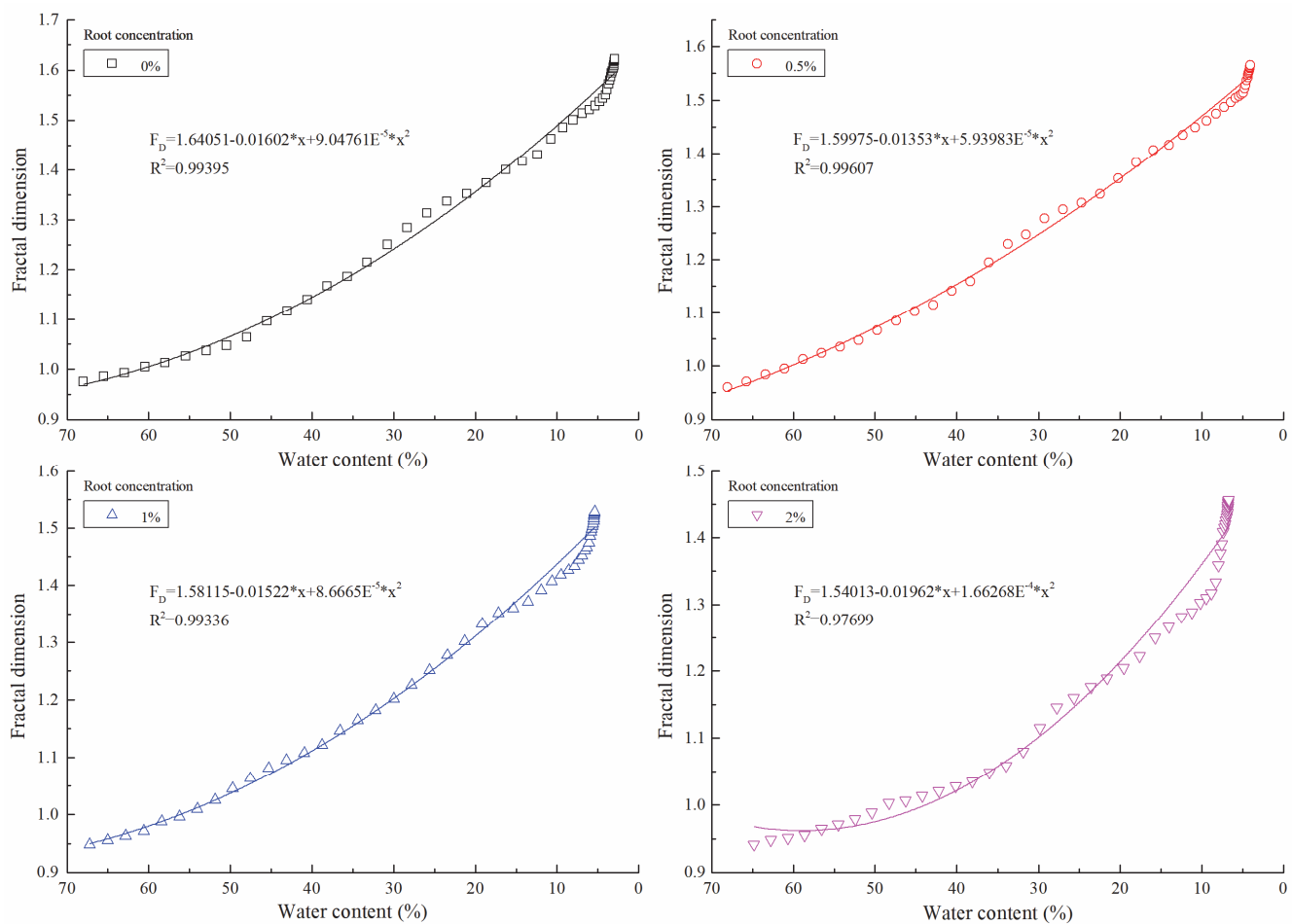
Figure 7. Relationship between water content and fractal dimension.

5. Conclusions

In this paper, 0%, 0.5%, 1%, and 2% hippophae roots additives were added to Saline-Alkali soil to study the effects of hippophae roots on evaporation and cracking of Saline-Alkali soil. Using ImageJ software transformations of pictures of soil sample cracks, the parameters of fractal dimension and crack ratio were quickly obtained. The relationships between fractal dimension and crack ratio and fractal dimension and water content were analyzed. The results are as follows:

(1) Residual water content decreased with a decrease in hippophae roots concentration. The residual water content of Saline-Alkali soil samples with 0%, 0.5%, 1%, and 2% concentrations of hippophae roots were 2.887%, 4.086%, 5.366%, and 6.696%, respectively.

(2) The cracking degree of Saline-Alkali soil samples was negatively related to the concentration of hippophae roots in the experiment. The final crack ratios of Saline-Alkali soil samples with hippophae root concentrations of 0.5%, 1%, and 2% were reduced by 4.87%, 11.29%, and 19.49%, respectively, compared with that of the soil sample without hippophae root.

(3) The addition of roots to Saline-Alkali soil effectively reduced the fractal dimension of final cracks. The fractal dimensions of Saline-Alkali soil samples containing 0%, 0.5%, 1%, and 2% at the end of cracking were 1.6217, 1.5656, 1.5282, and 1.4568, respectively.

(4) The fractal dimension increased with an increase in the crack ratio, which indicates a positive correlation. The fractal dimension increased with a decrease in water content; the relationship between fractal dimension and water content is a quadratic function.

References

1. Gholizadeh, A.; Kopačková, V. Detecting vegetation stress as a soil contamination proxy: A review of optical proximal and remote sensing techniques. *Int. J. Environ. Sci. Technol.* **2019**, *16*, 2511–2524. [CrossRef]
2. Abou Samra, R.M.; Ali, R.R. The development of an overlay model to predict soil salinity risks by using remote sensing and GIS techniques: A case study in soils around Idku Lake, Egypt. *Environ. Monit. Assess.* **2018**, *190*, 706. [CrossRef] [PubMed]
3. Chen, W.; Hou, Z.; Wu, L.; Liang, Y.; Wei, C. Evaluating salinity distribution in soil irrigated with saline water in arid regions of northwest China. *Agric. Water Manag.* **2010**, *97*, 2001–2008. [CrossRef]
4. Wichelns, D.; Qadir, M. Achieving sustainable irrigation requires effective management of salts, soil salinity, and shallow groundwater. *Agric. Water Manag.* **2015**, *157*, 31–38. [CrossRef]
5. Xing, X.G.; Kang, D.G.; Ma, X.Y. Differences in loam water retention and shrinkage behavior: Effects of various types and concentrations of salt ions. *Soil Till. Res.* **2017**, *167*, 61–72. [CrossRef]
6. Brown, C.E.; Pezeshki, S.R.; Delaune, R.D. The effects of salinity and soil drying on nutrient uptake and growth of *Spartina alterniflora* in a simulated tidal system. *Environ. Exp. Bot.* **2006**, *58*, 140–148. [CrossRef]
7. Dodd, K.; Guppy, C.N.; Lockwood, P.V.; Rochester, I.J. The effect of sodicity on cotton: Does soil chemistry or soil physical condition have the greater role? *Crop Pasture Sci.* **2013**, *64*, 806–815. [CrossRef]
8. Qadir, M.; Oster, J.D. Crop and irrigation management strategies for saline-sodic soils and waters aimed at environmentally sustainable agriculture. *Sci. Total Environ.* **2004**, *323*, 1–19. [CrossRef]
9. Crescimanno, G.; Santis, A.D. Bypass flow, salinization and sodication in a cracking clay soil. *Geoderma* **2004**, *121*, 307–321. [CrossRef]
10. Crescimanno, G.; Garofalo, P. Management of irrigation with saline water in cracking clay soils. *Soil Sci. Soc. Am. J.* **2006**, *70*, 1774–1787. [CrossRef]
11. Mahmoud, M.; Janssen, M.; Haboub, N.; Nassour, A.; Lennartz, B. The impact of olive mill wastewater application on flow and transport properties in soils. *Soil Till. Res.* **2010**, *107*, 36–41. [CrossRef]
12. Decarlo, K.F.; Shokri, N. Salinity effects on cracking morphology and dynamics in 3-D desiccating clays. *Water Resour. Res.* **2014**, *50*, 3052–3072. [CrossRef]
13. Levy, J.; Fountain, A.; Lyons, W.B.; Welch, K. Experimental formation of pore fluids in McMurdo Dry Valleys soils. *Antarct. Sci.* **2015**, *27*, 163–171. [CrossRef]
14. Ren, J.H.; Li, X.J.; Zhao, K.; Fu, B.L.; Jiang, T. Study of an on-line measurement method for the salt parameters of soda-saline soils based on the texture features of cracks. *Geoderma* **2016**, *263*, 60–69. [CrossRef]
15. Ren, J.H.; Zhao, K.; Wu, X.W.; Zheng, X.M.; Li, X.J. Comparative Analysis of the Spectral Response to Soil Salinity of Saline-Sodic Soils under Different Surface Conditions. *Int. J. Env. Res. Public Health* **2018**, *15*, 2721. [CrossRef] [PubMed]
16. Zhang, X.; Chen, Y.; Ye, W.; Cui, Y.; Deng, Y.; Chen, B. Effect of salt concentration on desiccation cracking behavior of GMZ bentonite. *Environ. Earth Sci.* **2017**, *76*, 531. [CrossRef]
17. Zhang, T.W.; Deng, Y.F.; Cui, Y.J.; Lan, H.X.; Zhang, F.Y.; Zhang, H.Y. Porewater salinity effect on flocculation and desiccation cracking behaviour of kaolin and bentonite considering working condition. *Eng. Geol.* **2019**, *251*, 11–23. [CrossRef]
18. Tran, D.; Ralaizafisoloarivony, N.; Charlier, R.; Mercatoris, B.; Léonard, A.; Toye, D.; Degré, A. Studying the effect of desiccation cracking on the evaporation process of a Luvisol—From a small-scale experimental and numerical approach. *Soil Till. Res.* **2019**, *193*, 142–152. [CrossRef]
19. Zhang, Y.; Ye, W.; Chen, B.; Chen, Y.; Ye, B. Desiccation of NaCl-contaminated soil of earthen heritages in the Site of Yar City, northwest China. *Appl. Clay Sci.* **2016**, *124–125*, 1–10. [CrossRef]
20. Dos Santos, J.; de Andrade, E.; Guerreiro, M.; Medeiros, P.; de Queiroz Palácio, H.; de Araújo Neto, J. Effect of dry spells and soil cracking on runoff generation in a semiarid micro watershed under land use change. *J. Hydrol.* **2016**, *541*, 1057–1066. [CrossRef]
21. Kurtzman, D.; Baram, S.; Dahan, O. Soil-aquifer phenomena affecting groundwater under vertisols: A review. *Hydrol. Earth Syst. Sci.* **2016**, *20*, 1–12. [CrossRef]

22. Rayhani, M.; Yanful, E.; Fakher, A. Desiccation-induced cracking and its effect on the hydraulic conductivity of clayey soils from Iran. *Can. Geotech. J.* **2007**, *44*, 276–283. [CrossRef]
23. Abd El-Halim, A. Image processing technique to assess the use of sugarcane pith to mitigate clayey soil cracks: Laboratory experiment. *Soil Till. Res.* **2017**, *169*, 138–145. [CrossRef]
24. Baer, J.; Kent, T.; Anderson, S. Image analysis and fractal geometry to characterize soil desiccation cracks. *Geoderma* **2009**, *154*, 153–163. [CrossRef]
25. Sun, D.; Wang, L.; Li, L. Stability of Unsaturated Soil Slopes with Cracks under Steady-Infiltration Conditions. *Int. J. Geomech.* **2019**, *19*, 04019044. [CrossRef]
26. Zhang, J.; Zhu, D.; Zhang, S. Shallow slope stability evolution during rainwater infiltration considering soil cracking state. *Comput. Geotech.* **2020**, *117*, 103285. [CrossRef]
27. Mostafazadeh-Fard, B.; Jafari, F.; Mousavi, S.; Yazdani, M. Effects of irrigation water management on yield and water use efficiency of rice in cracked paddy soils. *Aust. J. Crop Sci.* **2010**, *4*, 136–141.
28. Bayat, H.; Neyshaburi, M.; Mohammadi, K.; Nariman-Zadeh, N.; Irannejad, M.; Gregory, A. Combination of artificial neural networks and fractal theory to predict soil water retention curve. *Comput. Electron. Agric.* **2013**, *92*, 92–103. [CrossRef]
29. Mohammadi, M.; Shabanpour, M.; Mohammadi, M.H.; Davatgar, N. Characterizing Spatial Variability of Soil Textural Fractions and Fractal Parameters Derived from Particle Size Distributions. *Pedosphere* **2019**, *29*, 224–234. [CrossRef]
30. Zhang, Y.; Zhong, X.; Lin, J.; Zhao, D.; Jiang, F.; Wang, M.; Ge, H.; Huang, Y. Effects of fractal dimension and water content on the shear strength of red soil in the hilly granitic region of southern China. *Geomorphology* **2020**, *351*, 106956. [CrossRef]
31. Xu, Q.; Xiong, K.; Chi, Y. Effects of Intercropping on Fractal Dimension and Physicochemical Properties of Soil in Karst Areas. *Forests* **2021**, *12*, 1422. [CrossRef]
32. Lu, S.; Tang, H.; Zhang, Y.; Gong, W.; Wang, L. Effects of the particle-size distribution on the micro and macro behavior of soils: Fractal dimension as an indicator of the spatial variability of a slip zone in a landslide. *Bull. Eng. Geol. Environ.* **2018**, *77*, 665–677.
33. Preston, S.; Griffiths, B.; Young, I. An investigation into sources of soil crack heterogeneity using fractal geometry. *Eur. J. Soil Sci.* **1997**, *48*, 31–37. [CrossRef]
34. Collins, T.J. ImageJ for microscopy. *Biotechniques* **2007**, *43*, S25–S30. [CrossRef]
35. Yang, R.; He, S.; Yi, J.Z.; Hu, Q.H. Nano-scale pore structure and fractal dimension of organic-rich Wufeng-Longmaxi shale from Jiaoshiba area, Sichuan Basin: Investigations using FE-SEM, gas adsorption and helium pycnometry. *Mar. Petrol Geol.* **2016**, *70*, 27–45. [CrossRef]
36. Xu, L.F.; Zhang, J.C.; Ding, J.H.; Liu, T.; Shi, G.; Li, X.Q.; Dang, W.; Cheng, Y.S.; Guo, R.B. Pore Structure and Fractal Characteristics of Different Shale Lithofacies in the Dalong Formation in the Western Area of the Lower Yangtze Platform. *Minerals* **2020**, *10*, 72. [CrossRef]
37. Alruwaily, Y.; Ahmad, B.; Ntouyas, S.K.; Alzaidi, A.S.M. Existence results for coupled nonlinear sequential fractional differential equations with coupled Riemann-Stieltjes integro-multipoint boundary conditions. *Fractal Fract.* **2022**, *6*, 123. [CrossRef]
38. Owolabi, K.M.; Atangana, A.; Akgul, A. Modelling and analysis of fractal-fractional partial differential equations: Application to reaction-diffusion model. *Alex Eng. J.* **2020**, *59*, 2477–2490. [CrossRef]
39. Evagelopoulos, V.; Zoras, S.; Triantafyllou, A.G.; Albanis, T.A. PM10-PM2. 5 time series and fractal analysis. *Global Nest J.* **2006**, *8*, 234–240.
40. Yang, B.B.; Liu, Y. Application of fractals to evaluate fractures of rock due to mining. *Fractal Fract.* **2022**, *6*, 96. [CrossRef]
41. Asadi, H.H.; Kianpouryan, S.; Lu, Y.J.; McCuaig, T.C. Exploratory data analysis and C-A fractal model applied in mapping multi-element soil anomalies for drilling: A case study from the Sari Gunay epithermal gold deposit, NW Iran. *J. Geochem. Explor.* **2014**, *145*, 233–241. [CrossRef]
42. Li, C.J.; Ma, T.H.; Shi, J.F. Application of a fractal method relating concentrations and distances for separation of geochemical anomalies from background. *J. Geochem. Explor.* **2003**, *77*, 167–175. [CrossRef]
43. Ergün, S.; Saraçoglu, A.; Guneri, P.; Ozpınar, B. Application of fractal analysis in hyperparathyroidism. *Dentomaxillofac. Rad.* **2009**, *38*, 281–289. [CrossRef] [PubMed]
44. Gao, G.L.; Ding, G.D.; Zhao, Y.Y.; Wu, B.; Zhang, Y.Q.; Qin, S.G.; Bao, Y.F.; Yu, M.H.; Liu, Y.D. Fractal approach to estimating changes in soil properties following the establishment of Caragana korshinskii shelterbelts in Ningxia, NW China. *Ecol. Indic.* **2014**, *43*, 236–243. [CrossRef]
45. Li, Z.F.; Wang, Z.M. Experimental study on the relation between the fractal characteristics and solute transport parameters of sandy soil. *J. Soil Sediment* **2020**, *20*, 3181–3191. [CrossRef]
46. Cumbrera, R.; Tarquis, A.M.; Gascó, G.; Millán, H. Fractal scaling of apparent soil moisture estimated from vertical planes of Vertisol pit images. *J. Hydrol.* **2012**, *452*, 205–212. [CrossRef]
47. Chen, Y.; Yeh, H.; Gui, M.; Wei, C.; He, C. Estimation of surface soil moisture content using fractals. *Environ. Monit. Assess.* **2021**, *193*, 91. [CrossRef]